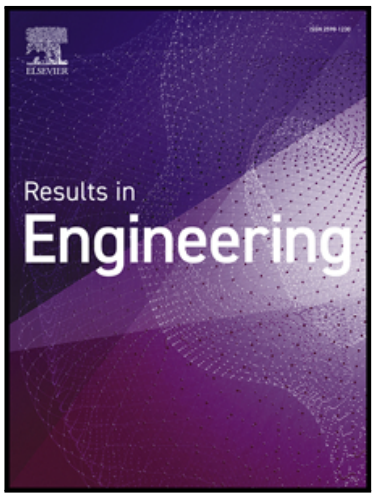

6G mm-Wave Nolen-Matrix Beamformer Using Groove Gap-Waveguide Technology for Tracking Space Targets and Satellite Global Connectivity Through IoT

Mohammad Alibakhshikenari , Bal Virdee ,
Yazeed Mohammad Qasaymeh , Nisar Ahmad Abbasi ,
Francisco Falcone , Takfarinas Saber , Ernesto Limiti

PII: S2590-1230(26)01607-5
DOI: https://doi.org/10.1016/j.rineng.2026.110572
Reference: RINENG 110572

To appear in: *Results in Engineering*

Received date: 4 April 2026
Accepted date: 15 April 2026

Please cite this article as: Mohammad Alibakhshikenari , Bal Virdee , Yazeed Mohammad Qasaymeh , Nisar Ahmad Abbasi , Francisco Falcone , Takfarinas Saber , Ernesto Limiti , 6G mm-Wave Nolen-Matrix Beamformer Using Groove Gap-Waveguide Technology for Tracking Space Targets and Satellite Global Connectivity Through IoT, *Results in Engineering* (2026), doi: https://doi.org/10.1016/j.rineng.2026.110572

Highlights

- This work introduces an innovative 3×3 beamforming Nolen-matrix feeding network utilizing gap-waveguide technology.
- The innovation lies in the matrix's crossover-free architecture.
- The system's performance is experimentally validated over the entire 36–39 GHz band.
- The proposed beamformer represents a highly efficient and robust solution for next-generation beamforming arrays and 6G mm-wave satellite communications.

6G mm-Wave Nolen-Matrix Beamformer Using Groove Gap-Waveguide Technology for Tracking Space Targets and Satellite Global Connectivity Through IoT

Mohammad Alibakhshikenari[1,2]*, Bal Virdee[3], Yazeed Mohammad Qasaymeh[4]*, Nisar Ahmad Abbasi[5], Francisco Falcone[6], Takfarinas Saber[1], and Ernesto Limiti[7]

[1]Lero, the Research Ireland Centre for Software, College of Science and Engineering, School of Computer Science, University of Galway, H91 TK33 Galway, Ireland; mohammad.alibakhshikenari@universityofgalway.ie, takfarinas.saber@universityofgalway.ie

[2]Department of Electrical and Electronics Engineering, Dogus University, 34775 Umraniye, Istanbul, Türkiye.

[3]Center for Communications Technology, London Metropolitan University, London N7 8DB, United Kingdom; b.virdee@londonmet.ac.uk

[4]Department of Electrical and Electronics Engineering, College of Engineering, Majmaah University, Majmaah, 11952, Saudi Arabia; y.qasaymeh@mu.edu.sa

[5]Department of Electrical Engineering, School of Systems Engineering, Bahrain Polytechnic, 33349 Isa Town, Bahrain; nisar.abbasi@polytechnic.bh

[6]nstitute of Smart Cities, Department of Electric, Electronic and Communication Engineering, Public University of Navarre, 31006 Pamplona, Spain; francisco.falcone@unavarra.es

[7]Electronics Engineering Department, University of Rome "Tor Vergata", 00133 Rome, Italy; limiti@ing.uniroma2.it

**Corresponding authors: Mohammad Alibakhshikenari, and Yazeed Mohammad Qasaymeh*

***Abstract*: This paper presents a compact 3×3 beamforming Nolen-matrix feeding network (BNMFN) based on groove gap-waveguide (GGW) technology for Ka-band satellite and space-multiplexing applications. The proposed design eliminates conventional components such as power dividers, crossovers, switches, and terminations by utilizing only directional couplers and phase-shift compensators, thereby reducing size, loss, and complexity. The network employs three 90° couplers (3.14 dB and 4.84 dB) and two-phase shifters (–38° and –63°) to achieve output phase differences of 270°, 30°, and 150° at 38 GHz. Integrated with a GGW-based feeding transition and a three-element slotted antenna array, the system demonstrates multi-beam radiation with gains exceeding 17 dBi over 36–39 GHz. Experimental results validate low loss, wide bandwidth, and accurate phase performance, making the design a promising solution for 6G millimeter-wave satellite communications and IoT connectivity.**

***Keywords*: Beamforming Nolen-matrix feeding network, groove gap-waveguide technology, mm-wave systems, antenna array, space-multiplexing, satellite connectivity, Internet of Things (IoT).**

I. INTRODUCTION

The rapid growth in satellite communication systems has significantly increased the demand for high-performance technologies operating in the millimeter-wave (mm-wave) spectrum [1]. This frequency band is favoured due to its broad bandwidth, expansive spectrum availability, and ability to support miniaturized antennas and circuits, which are essential for modern wireless front-end systems [2]. To meet these demands, millimeter-wave circuits and modules must exhibit high efficiency, low loss, and cost-effective implementation [3,4].

A critical technique for enhancing the spectral efficiency of mm-wave satellite systems is space multiplexing. This method improves channel capacity and mitigates issues such as multipath fading and co-channel interference [5]. Central to space multiplexing is the use of beamforming feeding networks (BFNs), which control the amplitude and phase of signals across antenna arrays to enable beam steering and switching [6,7]. Common BFN architectures include series-feed, parallel-feed, and matrix feeding configurations [8].

Series and parallel feed networks, such as Luneburg, Ruze, and Rotman lenses [9,10], often require a large number of phase shifters with broad tuning ranges. These lens-based systems typically suffer from phase errors that limit beamforming precision, bandwidth, and scanning angles. Additionally, they face challenges such as bulky structures, high insertion losses, and complex, non-planar designs—making them less suitable for compact and multi-beam MIMO systems.

By contrast, matrix feeding networks offer a more compact, scalable, and efficient alternative. These systems consist of couplers, phase shifters, power dividers, and switches, and are particularly attractive for MIMO-enabled phased arrays [11,12]. Among the popular matrix-based designs are the Blass, Butler, and Nolen matrices, known for their reduced size, lower losses, and simpler configurations compared to lens-based approaches [13,14].

The Butler matrix is widely used due to its symmetric layout and ability to generate progressive phase shifts and equal amplitudes at its outputs when any one of its input ports is excited [15–17]. The Blass matrix, introduced earlier, operates similarly but suffers from reduced efficiency due to power dissipation in termination loads [18]. To overcome these losses, the Nolen matrix was developed. It improves upon the Blass design by halving its structure along the diagonal and replacing diagonal couplers with phase delay lines, resulting in a more efficient and compact configuration [19,20]. Both Butler and Nolen matrices are preferred for their simplicity, lossless behaviour, broad bandwidth, and absence of crossover lines particularly the Nolen matrix, which achieves equivalent functionality with fewer components and no crossovers [21–27].

Traditionally, these matrices have been implemented using technologies like printed circuit boards (PCBs), microstrip lines, substrate integrated waveguides (SIWs), and metallic waveguides [28–31]. However, such implementations often suffer from dielectric and radiation losses, especially at mm-wave frequencies, limiting their bandwidth and performance. For example, SIWs are hard to integrate into planar base station layouts and struggle to maintain low loss and wide bandwidth simultaneously.

To address these limitations, gap-waveguide transmission line (GW-TL) technology has emerged as a compelling alternative. It supports low-loss, wideband, and leakage-free signal propagation by guiding waves through an air-filled gap bordered by periodic metallic structures that mimic perfect magnetic conductor (PMC) behaviour [32,33]. This makes GW-TL ideal for implementing high-efficiency feeding networks in the mm-wave regime.

In this research, we propose a 3×3 beamforming Nolen-matrix feeding network (BNMFN) leveraging groove gap-waveguide (GGW) technology. The matrix consists of three 90° directional couplers with two specific coupling ratios and two custom-designed phase shifters, all constructed using periodic metallic pins. This design eliminates unnecessary components like power dividers, crossovers, and terminations, offering a compact, efficient, and low-loss beamforming solution suitable for Ka-band satellite communication and 5G/6G applications. Additionally, the matrix is integrated with a slotted antenna array and input feeding transition, making it a practical and scalable solution for real-world deployment in space-multiplexed systems.

II. GW-BASED UNIT-CELL

To realize a high-performance beamforming network based on groove gap-waveguide (GGW) technology, a unit-cell is first designed to support a wide electromagnetic stopband across the desired frequency range. This unit-cell serves as the fundamental building block for implementing waveguiding structures such as directional couplers and phase shifters.

The concept is based on gap-waveguide (GW) technology, where electromagnetic propagation is controlled using a parallel-plate configuration with one surface engineered to behave as a perfect magnetic conductor (PMC). When the gap is smaller than a quarter-wavelength ($\lambda/4$), wave propagation is suppressed outside the guiding region [32].

Periodic metallic pin structures (artificial magnetic conductors) are used to realize the PMC behavior required for GW operation [33]. These pins prevent unwanted wave propagation, while the introduction of a PEC ridge or groove between them forms a confined, low-loss propagation path. This configuration provides low radiation loss and high isolation, making it suitable for mm-wave applications.

The electromagnetic behavior of the unit-cell is determined by key geometrical parameters, including the pin height (h), period (p), width (w), and the gap distance (d), which is maintained

below λ/4 to ensure stopband operation. These parameters are optimized for Ka-band operation centered at 38 GHz, as summarized in Table I.

The dispersion diagram in Fig. 1 confirms a wide stopband covering 21–39 GHz, ensuring effective suppression of unwanted propagation modes. This validates the unit-cell design for use in GGW-based components such as the 90° directional couplers and phase-shift compensators employed in the proposed beamforming network.

The next design step involves applying this unit-cell structure to construct groove gap-waveguide-based directional couplers and phase shifters, which serve as the core elements of the proposed beamforming Nolen-matrix feeding network.

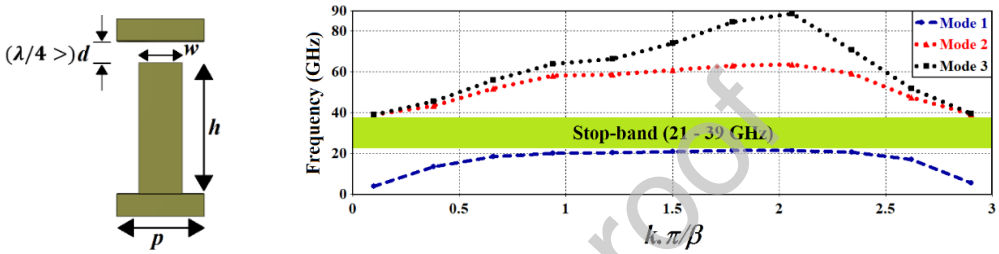

(a) (b)

Fig.1. Unit-cell, (a) layout, and (b) dispersion diagram.

TABLE I. DIMENSIONS OF THE UNIT-CELL AT 38 GHz

Parameter	Value (mm)
h	3
p	2
d	0.5 < λ/4
w	1

III. BEAMFORMING NOLEN-MATRIX FEEDING NETWORK

The design of a beamforming Nolen-matrix feeding network (BNMFN) aims to provide simultaneous multi-beam radiation with low loss and compact size, making it ideal for millimeter-wave applications such as satellite and 5G systems. A schematic of the proposed 3×3 BNMFN is shown in Fig. 2(a). The matrix consists of three input ports (P1–P3) and three output ports (P4–P6). The architecture employs one coupler with a coupling ratio of CR1 = 2/3 placed at the top and two couplers with a coupling ratio of CR2 = 1/2 arranged at the bottom.

The selected coupling ratios are determined by the equal-amplitude condition of the 3×3 Nolen-matrix topology. In the first stage, one coupler must extract one-third of the input power toward one output branch while allowing the remaining two-thirds to propagate to the second

stage. This corresponds to an ideal coupling level of $10\log_{10}(3) \approx 4.77$ dB, which is realized as 4.84 dB at 38 GHz after full-wave optimization in the GGW implementation.

The remaining power is then equally divided between the two lower branches using two identical couplers, requiring an ideal 3 dB split, which is realized as 3.14 dB at 38 GHz.

In addition to amplitude control, the phase response is governed by the intrinsic 90° phase difference of the directional couplers and the incorporation of phase-shift compensators. The two compensators, providing −63° and −38° phase shifts, are introduced to correct the phase imbalance caused by unequal signal paths.

As a result, the combined effect of the coupling ratios and phase compensation enables the required output phase differences of approximately 270°, 30°, and 150° at the three output ports, with simulated results closely matching the theoretical targets. The parallel topology further ensures minimal signal interference and supports broad bandwidth operation.

To deliver optimal signal performance at high frequencies, all structural components are implemented using Groove Gap-Waveguide (GGW) technology, which suppresses unwanted propagation modes and avoids dielectric losses through the use of periodic metallic pins [32,33]. The GGW design eliminates the need for crossovers, load terminations, and power dividers, making it more efficient than conventional Blass and Butler matrices [19–22].

In this configuration, each input generates three signals of equal magnitude but with specific phase differences at the output ports. The matrix is engineered so that the output phase shifts between ports P4, P5, and P6 are approximately 270°, 30°, and 150°, respectively. To achieve these values, custom phase-shift compensators are integrated to fine-tune the overall phase response, as discussed later.

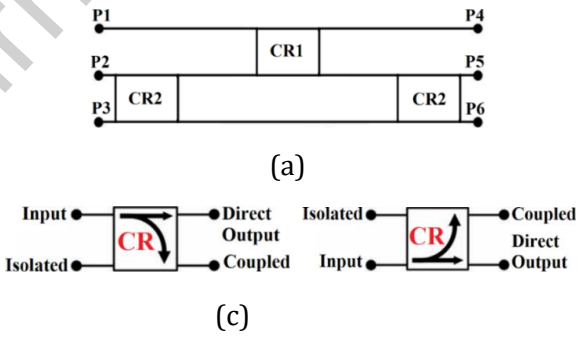

Fig.2. (a) Schematic diagram of the standard 3×3 Nolen matrix. The characteristics for couplers required in the proposed feeding network (b) exciting input from the top, and (c) exciting input from the bottom.

A) Implementation of the Directional 90° Coupler

The BNMFN relies on directional couplers to distribute input signals with controlled amplitude and phase. Two types of GGW-based 90° directional couplers are designed with coupling ratios of 3.14 dB and 4.84 dB. The layout of these four-port couplers is presented in Fig.

3(a), where ports 1–4 correspond to the input, direct output, coupled output, and isolated port, respectively.

The geometrical parameters of the couplers, critical to achieving the desired coupling ratios, are summarized in Table II. Among these, the spacing "S_1 & S_2") play the most significant role in defining the coupling level. Other structural dimensions are consistent with the unit-cell configuration detailed earlier in Table I.

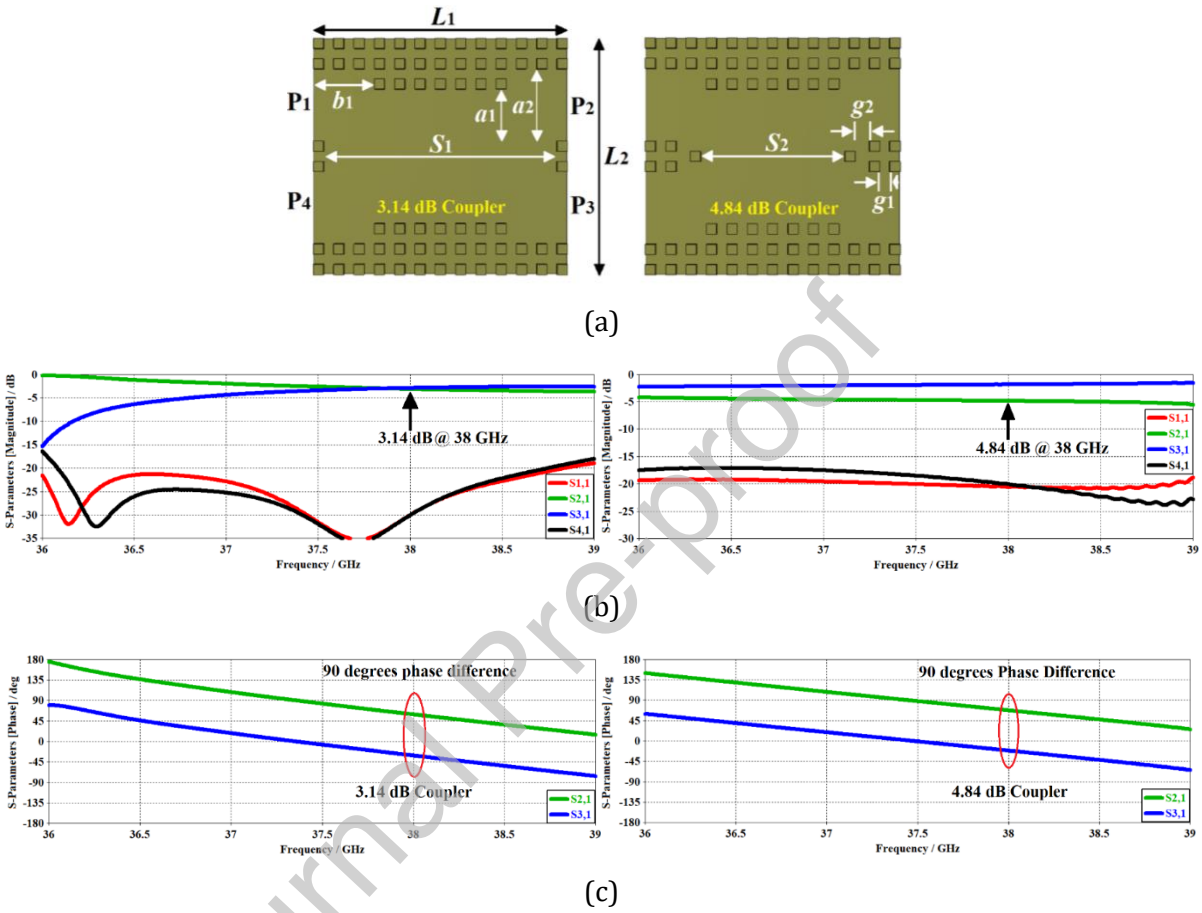

Fig.3. Four-ports directional 90° couplers with two coupling ratios of 3.14- and 4.84-dB at 38 GHz, (a) layouts, (b) S-parameters, and (c) 90° phase difference between the direct output and coupled ports across entire band.

As shown in Fig. 3(b), both couplers exhibit excellent performance over the 36–39 GHz frequency range, with reflection coefficients and isolation better than –20 dB, and the desired coupling values achieved precisely at 38 GHz, a central frequency for 5G applications [1]. Fig. 3(c) confirms a consistent 90° phase shift between the direct and coupled ports across the entire operating band, validating the design's suitability for phase-array systems

TABLE II. DIMENSIONS OF THE DIRECTIONAL 90° COUPLERS

Parameter	Value (mm)
S_1	23

S_2	14.2
a_1	5.1
a_2	7.1
b_1	6
g_1	1
g_2	1.4
L_1	25
L_2	23.2

B) Designing the Phase-Shift Compensator

To ensure correct beamforming functionality, additional phase-shift compensators are required due to differing signal paths through the couplers. Specifically, signals routed from input Port 1 to output Ports P5 and P6 pass through both the 4.84 dB and 3.14 dB couplers, while the signal to P4 passes through only one coupler. This imbalance necessitates compensatory phase delays to equalize the cumulative phase shift.

As depicted in Fig. 4(a), two compensators introducing shifts of −63° (θ_1) and −38° (θ_2) are strategically placed within the network. These are realized by varying the widths of the waveguide sections ($w_1 \neq w_2$), as illustrated in Fig. 4(b). The optimized geometrical parameters of these phase-shifters are listed in Table III.

Simulation results shown in Fig. 4(c) confirm wideband operation from 36–39 GHz, with return losses better than −20 dB and nearly zero transmission loss. The resulting phase responses, plotted in Fig. 4(d), remain stable across the frequency band, delivering the designed phase shifts precisely at 38 GHz.

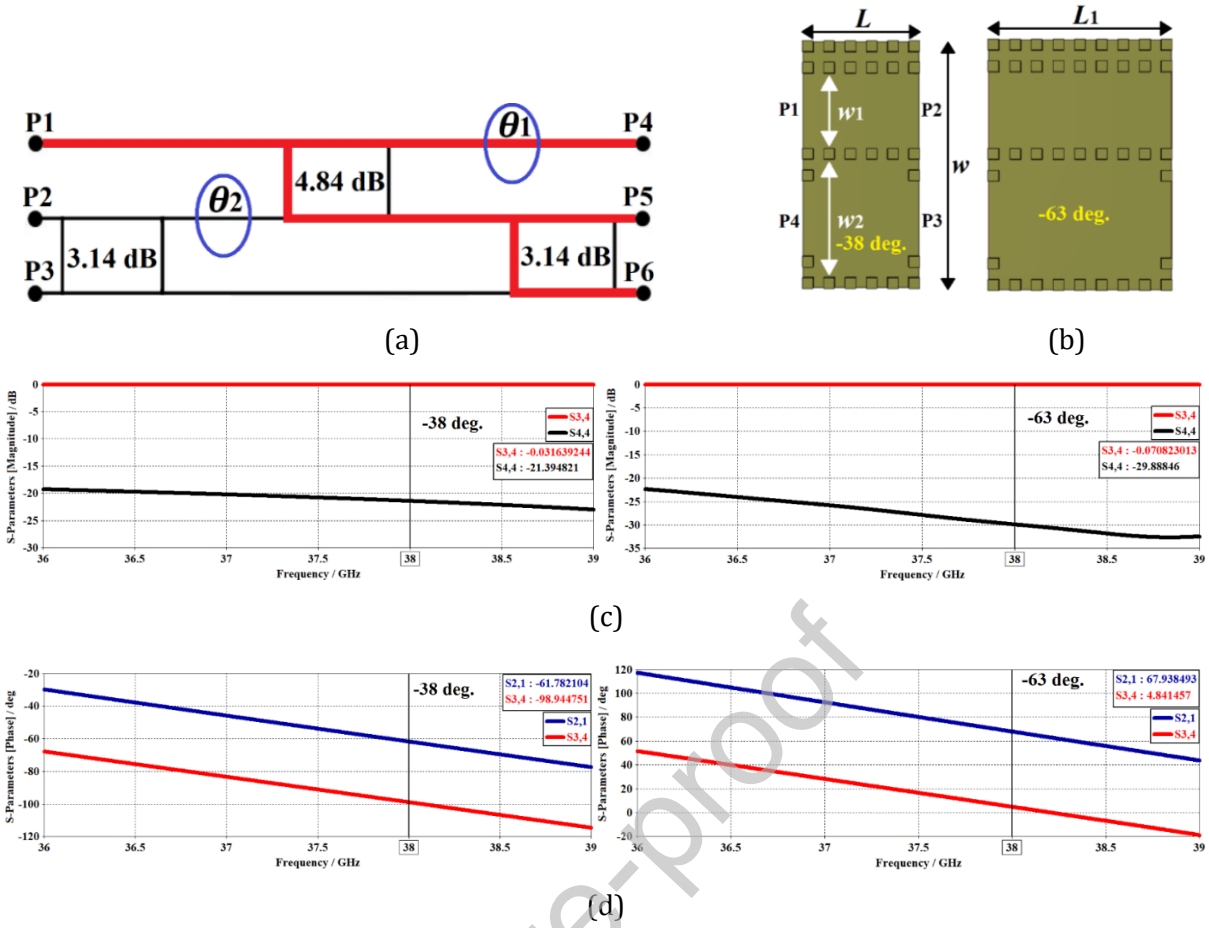

Fig.4. (a) Schematic diagram of the proposed 3×3 BNMFN, (b) layouts of the −38° and −63° phase-shift compensators, (c) reflection- and transmission-coefficients, and (d) phase-shift values.

TABLE III. DIMENSIONS OF THE PHASE-SHIFTERS

Parameter	Value (mm)
L	11
L1	17
w	23.2
w1	7.1
w2	11.1

C) Construction of the 3×3 BNMFN

The completed layout of the 3×3 BNMFN is presented in Fig. 5(a). It integrates three directional couplers and two phase-shift compensators using GGW techniques. The total dimensions of the matrix are 103 mm in length and 33.3 mm in width, emphasizing the compact nature of the design.

The S-parameter performance is detailed in Figs. 5(b) and 5(c). As shown, all input ports (P1–P3) maintain return-loss better than –15 dB across the entire 36–39 GHz range, with even better performance near the center frequency of 38 GHz. Isolation between input ports also exceeds 15 dB, while transmission magnitudes remain consistent at approximately 5 dB.

Importantly, the phase differences between successive output ports, which are critical for beamforming, closely match the theoretical values as follows:

- From P1: 268.5° and 269.5°
- From P2: 31° and 27.6°
- From P3: 148.5° and 148.5°

These results align closely with the target values of 270°, 30°, and 150°, confirming the network's suitability for multi-beam radiation.

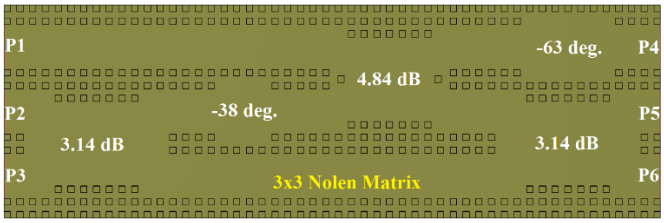

(a)

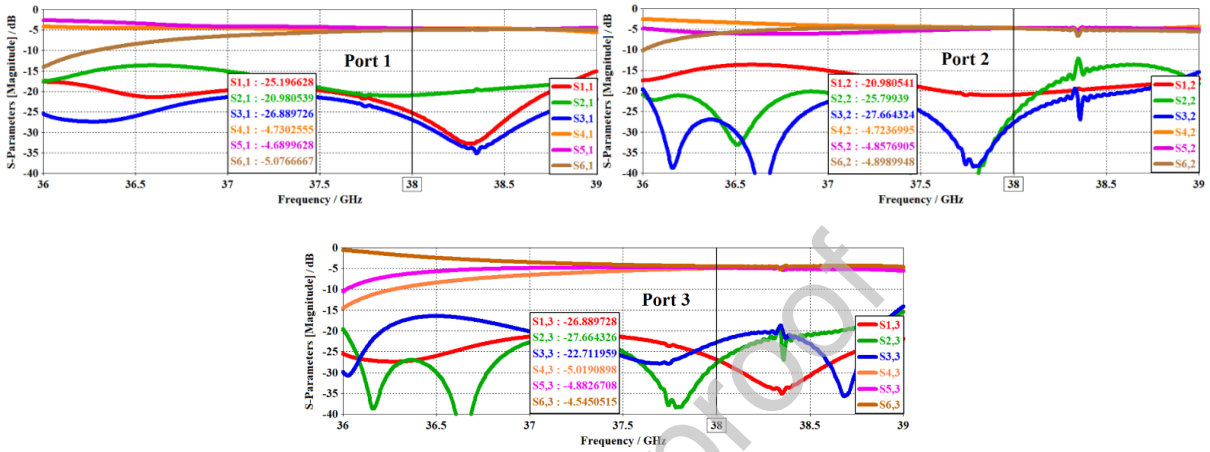

(b)

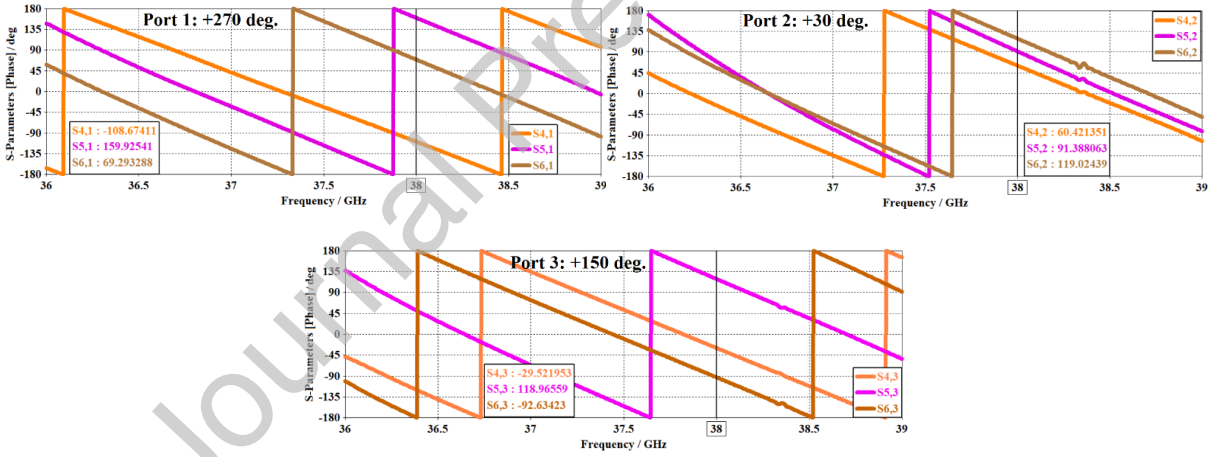

(c)

Fig.5. (a) Topology of the proposed 3×3 BNMFN, (b) S-parameter responses including reflection- and transmission-coefficients, & isolations between inputs, and (c) phase differences between each two consecutive output ports.

D) Realization of the Input Feeding Transition (IFT)

Although structurally simple, the input feeding transition (IFT) is essential for the overall system performance, as it ensures proper impedance matching, high isolation, and uniform amplitude and phase distribution between input ports, thereby enabling accurate excitation of the beamforming network at Ka-band frequencies.

To ensure compatibility with standard WR-28 waveguide flange adapters (covering 26.5–40 GHz), the IFT is developed to feed the BNMFN without introducing mismatches. The IFT increases spacing between input ports to accommodate mechanical constraints while maintaining electrical integrity.

The layout of the IFT is shown in Fig. 6(a). The design meets three critical conditions:

1. High return loss (better than –30 dB)
2. Excellent isolation (>80 dB between ports)
3. Equal transmission magnitude and phase among outputs

Performance plots in Fig. 6(b) confirm these metrics across 36–39 GHz. As shown in Fig. 6(c), phase differences between the outputs are negligible, ensuring consistent input excitation for the BNMFN.

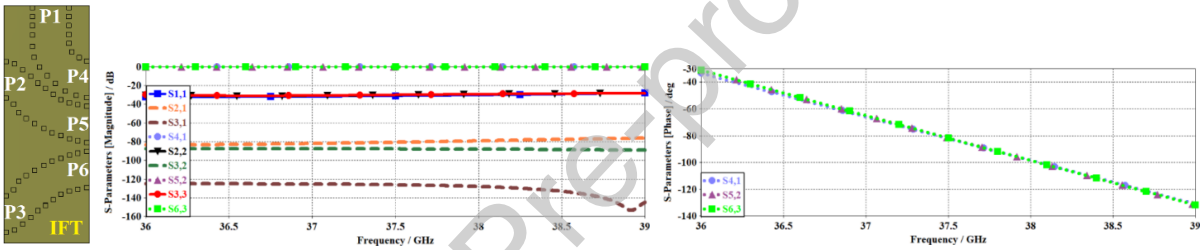

(a) (b) (c)

Fig.6. (a) Configuration of the proposed 3×3 input feeding transition (IFT), (b) reflection- and transmission-coefficients along with isolation between the inputs, and (c) phase differences between the outputs.

E) Integration of IFT and BNMFN

It should be noted that Fig. 5 presents the performance of the standalone BNMFN, whereas Fig. 7 illustrates the performance after integration with the input feeding transition (IFT). Although the responses appear similar, the comparison is intentionally included to demonstrate that the incorporation of the IFT does not degrade the electromagnetic performance of the beamforming network. In particular, the return loss, port isolation, and phase differences remain nearly unchanged after integration, confirming the robustness of the proposed design and the negligible impact of the IFT on system performance.

The complete integration of the IFT and BNMFN is displayed in Fig. 7(a). The combined system retains the performance of the individual components, as evidenced by the S-parameter plots in Figs. 7(b) and 7(c). The measured return-loss, isolation, and phase differences remain virtually unchanged after integration, validating the robustness of the design.

This fully integrated front-end structure enables the BNMFN to be fed with high-fidelity input signals and is ready for antenna array integration.

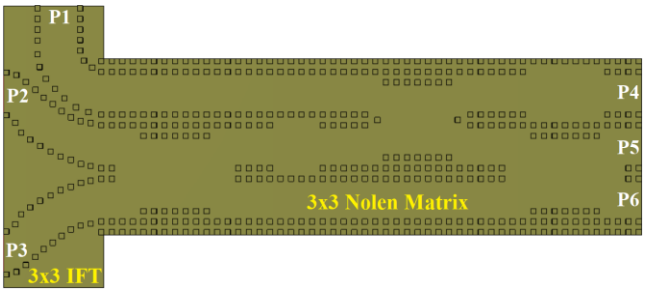

(a)

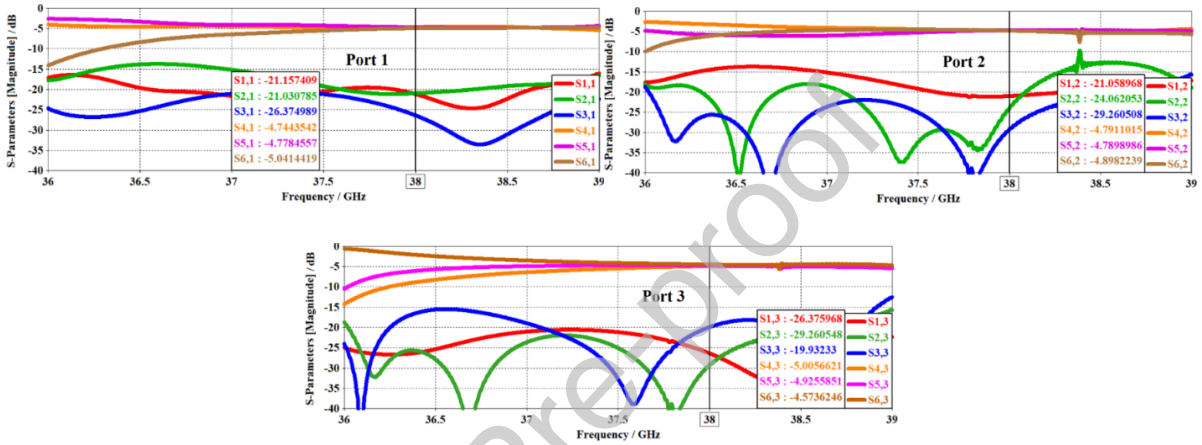

(b)

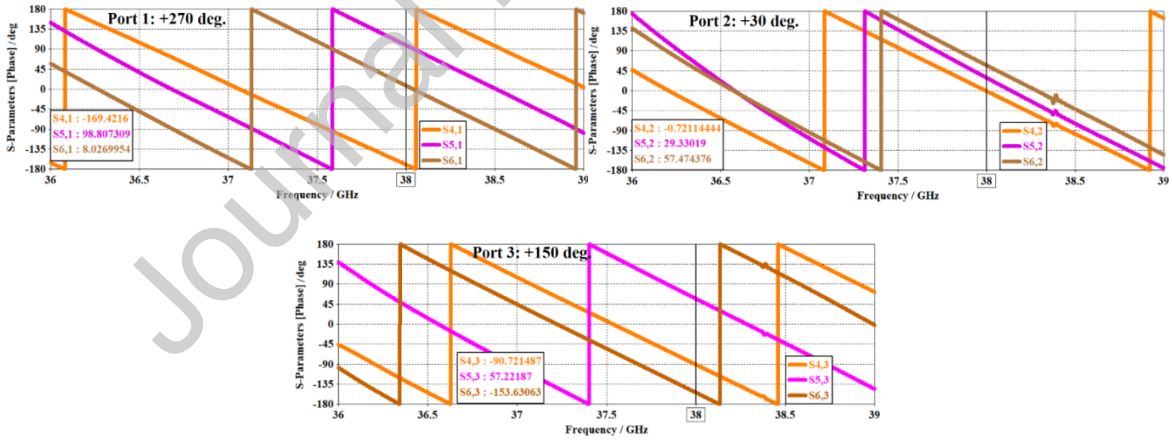

(c)

Fig.7. (a) Layout of the integrated structure (BNMFN+IFT), (b) reflection- and transmission-coefficients, & isolations between inputs, and (c) phase differences between each two consecutive output ports. These results are compared with Fig. 5 to verify that the inclusion of the IFT does not affect the BNMFN performance.

F) Slotted Antenna and Array Designs

To enable radiation capability, a slotted waveguide antenna based on Groove Gap-Waveguide (GGW) technology was designed and optimized to operate effectively across the Ka-band spectrum, specifically the 36–39 GHz range. The antenna layout is shown in Fig. 8(a). This structure preserves the same waveguide width as the previously discussed BNMFN and Input Feeding Transition (IFT), a critical design choice that ensures impedance matching and reduces reflection losses across interfaced components.

The slotted antenna consists of periodic radiating slots etched on the top surface of a GGW structure. These slots are spaced and sized to efficiently radiate guided energy into free space, forming a directive beam. The reflection coefficient (S_{11}) shown in Fig. 8(b) indicates excellent impedance matching, with values consistently below –20 dB across the desired frequency band. This reflects minimal power being reflected back to the source, which implies effective radiation and minimal mismatch.

A key performance metric for antennas is gain, which quantifies the antenna's ability to direct energy in a specific direction. The simulated realized gain pattern at 38 GHz is illustrated in Fig. 8(c). It reveals a peak gain of 19.65 dBi, indicating a strong and focused main beam ideal for point-to-point satellite links and other directive applications.

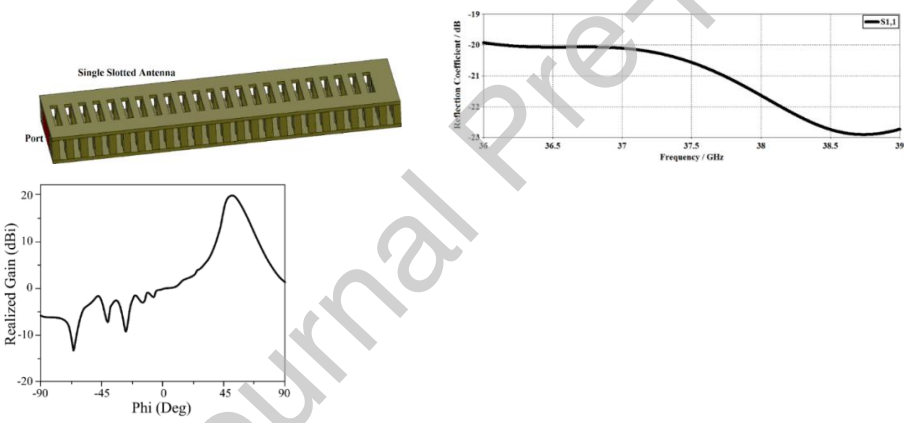

(a) (b)

(c)

Fig.8. (a) Layout of the single slotted antenna, (b) reflection coefficient, and (c) gain at 38 GHz.

To further enhance radiation performance and beamforming capability, the single-element slotted antenna was extended into a three-element linear antenna array, as shown in Fig. 9(a). This array configuration facilitates multi-beam operation, enabling the structure to support spatial multiplexing and angular separation of multiple communication channels, an essential requirement for modern satellite and MIMO systems.

The corresponding S-parameter plots in Fig. 9(b) demonstrate the effectiveness of this array configuration. The return loss for each element remains below –20 dB across the full operating band, reflecting good impedance matching. More importantly, the inter-element isolation exceeds

35 dB, ensuring minimal mutual coupling between adjacent elements. High isolation is crucial for beamforming networks to prevent interference and distortion between independent radiation paths.

It should be noted that the slotted antenna shown in Fig. 8 is a single radiating element and therefore does not exhibit beam-scanning by itself. Fig. 8 is included to validate the impedance matching and gain performance of the individual antenna prior to array formation. The beam-scanning functionality is realized only after integrating three such elements with the proposed BNMFN and input feeding transition, as shown in Fig. 10, where three distinct beams are obtained at approximately +53.0°, 0°, and −52.4° at 38 GHz.

G) Full Beamforming System Integration

To fully demonstrate the functionality of the proposed beamforming solution, the complete system comprising the IFT, 3×3 BNMFN, and the 1×3 Slotted Antenna Array, as shown in Fig. 10(a), was fabricated and tested. The physical realization of this integrated beamforming front-end is shown in Fig. 10(b). This structure maintains a compact and planar form factor, optimized for high-frequency operation while minimizing losses and interconnect complexity. WR-28 waveguide connectors are used to interface with standard measurement equipment, ensuring reliable excitation and data acquisition across all three input ports.

All measurements were conducted inside a fully shielded anechoic chamber, specifically designed to suppress unwanted reflections and eliminate external electromagnetic interference. This controlled environment ensures accurate assessment of the antenna's performance in terms of S-parameters and radiation characteristics across the 36–39 GHz frequency band.

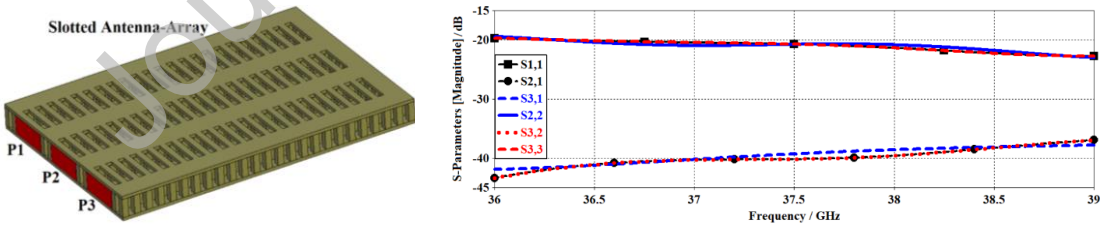

(a) (b)

Fig.9. (a) Configuration of the three-elements antenna array, and (b) reflection coefficients and the isolation between the input ports.

To facilitate precise alignment and reproducibility, the beamforming antenna was securely mounted on a motorized positioning stage. This setup allowed for controlled angular rotation and spatial alignment with respect to the measurement system, ensuring consistent orientation during radiation pattern acquisition.

The input ports of the beamforming network were excited via a WR28 waveguide-to-coaxial flange adapter, enabling efficient signal injection into the high-frequency system. The ports were excited sequentially or simultaneously to analyze the beamforming behavior under various input conditions. This approach allowed for comprehensive evaluation of inter-element coupling, port isolation, and beam steering capabilities.

A high-frequency vector network analyzer (VNA) was employed to measure the S-parameters of the beamforming network, providing detailed insights into input matching, insertion loss, and port-to-port isolation over the entire 36–39 GHz range. Calibration of the VNA was performed using a standard TRL (Thru-Reflect-Line) or SOLT (Short-Open-Load-Thru) method to eliminate systematic errors from cables and connectors.

The reflection and isolation characteristics of the system are presented in Fig. 10(c) for all three ports. Return losses (S_{11}, S_{22}, S_{33}) remain consistently below −15 dB across the operational band (36–39 GHz), confirming effective impedance matching for each feed port. Furthermore, inter-port isolation (S_{21}, S_{31}, S_{32}) exceeds 20 dB across most of the band and dips to values below −30 dB at the design frequency, which minimizes signal leakage and crosstalk which is critical for spatial multiplexing and multi-beam operation. These results confirm the array's ability to generate highly directive and well-isolated beams in distinct angular directions.

For far-field radiation measurements, a calibrated receiving antenna was placed at a fixed distance from the device under test (DUT) along the boresight direction. This receiving antenna captured the radiated fields, which were analyzed to extract radiation patterns, beam direction, and gain performance, thereby validating the beamforming functionality of the proposed design.

The integrated system was evaluated through both full-wave simulations and experimental measurements. The realized gain plots for input Ports P1, P2, and P3 are depicted in Fig. 10(d). These gain patterns confirm that the integrated structure produces three distinct radiation beams at 38 GHz, each with a main lobe directed at approximately +53°, 0°, and -52.4° and gain levels exceeding 17 dBi:

- Port P1: 17.37 dBi at +53.00°
- Port P2: 17.54 dBi at 0°
- Port P3: 17.43 dBi at –52.4°

These results indicate that the proposed beamforming system provides a wide beam scanning capability over –53° to +53°, which can be useful for satellite communications and space-multiplexing.

The measured results exhibit excellent agreement with simulated predictions, indicating high fabrication accuracy and design robustness. Slight variations between measured and simulated

curves, mostly in the sidelobe structure, are within acceptable limits for mm-wave implementations and are attributed to typical fabrication tolerances and connector alignment.

These measurements validate the system's ability to simultaneously radiate three high-gain beams with precise angular separation and minimal interference. The key performance indicators obtained from the measurements, including the directional characteristics of each port at 38 GHz, are summarized in Table IV, further confirming the suitability of the proposed design for Ka-band satellite communications and 5G/6G millimeter-wave front-end systems [2,27,35–38].

It should be noted that the radiated beams are not aligned with the broadside direction at 38 GHz. This is expected, as the proposed BNMFN introduces specific phase differences (270°, 30°, and 150°) between the output ports, resulting in beam steering toward different angular directions.

The radiation patterns were measured in a fully shielded anechoic chamber using a standard far-field measurement setup. The antenna under test (AUT) was mounted on a motorized rotation stage to enable precise angular scanning. A calibrated receiving antenna was positioned in the far-field region, and a vector network analyzer (Keysight N5247B) was used to measure the transmission characteristics. Each input port was excited individually through WR-28 waveguide interfaces, and the corresponding radiation patterns were recorded over the angular range. All measurements were performed after proper calibration to ensure accuracy. This setup ensures accurate characterization of the beam directions and gain performance of the proposed beamforming system.

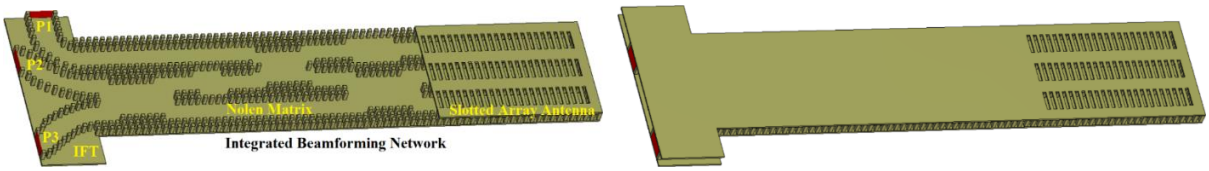

Top layer (hidden) Top layer (visible)

(a)

(b)

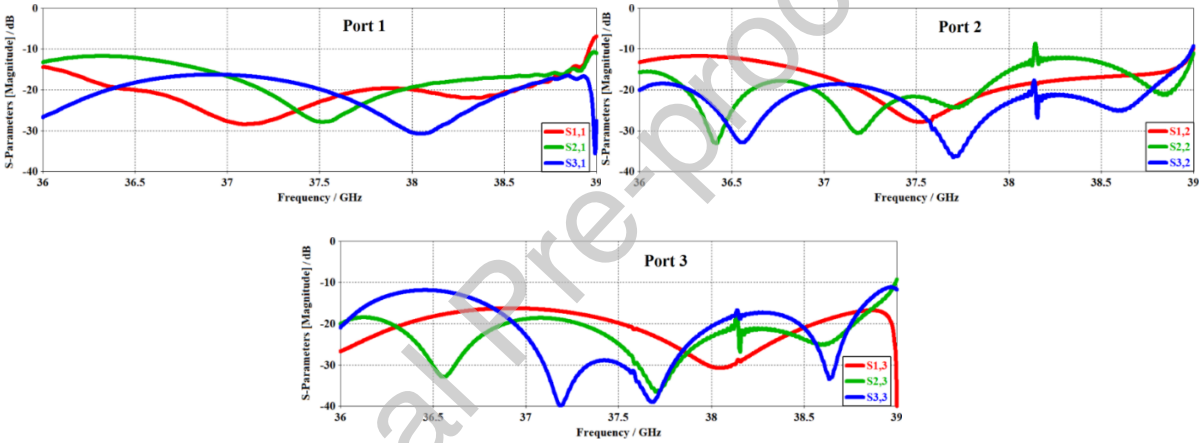

(c)

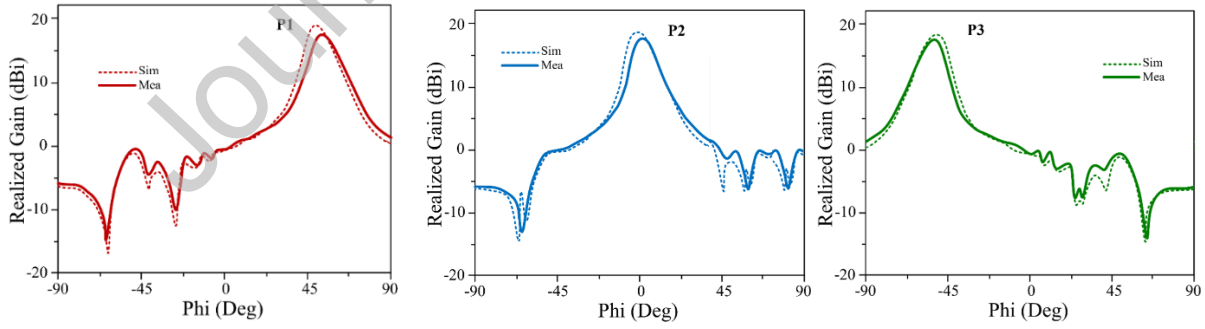

(d)

Fig.10. Configuration of the 3×3 GGW inspired integrated beamforming network, (a) simulated layout, (b) fabricated prototype, (c) measured reflection coefficient response and isolation between the ports, and (d) simulated and measured gain at the three ports at 38 GHz excited by the WR28 waveguide adapter.

TABLE IV. MEASURED PERFORMANCE PARAMETERS OF THE THREE-ELEMENT ANTENNA ARRAY

Measured	P1	P2	P3
Freq. (GHz)	38	38	38
Main lobe gain (dBi)	17.37	17.54	17.43
Main lobe direction (deg.)	+53.00	0.0	-52.40
Angular width (3 dB)	14.18	13.56	13.80
Side lobe (dB)	17.54	18.10	18.24

These results confirm the beamforming system's ability to support high-gain, multi-beam radiation with precise directionality and high port isolation, demonstrating its strong potential for integration into future space-multiplexed communication systems, phased arrays, and compact mm-wave satellite terminals.

The final integrated structure of the proposed system, shown in Fig. 10, illustrates the complete beamforming front-end composed of the 3×3 Input Feeding Transition, the Beamforming Nolen-Matrix Feeding Network, and the 1×3 slotted antenna array. This configuration highlights the compact, crossover-free, and modular nature of the design. It simplifies implementation and enhances scalability. The physical arrangement confirms the structural feasibility of the system for millimeter-wave applications, and validates its practical deployment in space-multiplexing and satellite communications for global IoT-based coverage, including applications such as smart transportation and traffic management, infrastructure and environmental (air and water quality) monitoring, public safety and surveillance, and smart energy distribution.

The proposed beamforming antenna is particularly suitable for space target tracking and satellite global connectivity applications. In tracking scenarios, the multi-beam capability enables simultaneous coverage over a wide angular range (approximately −53° to +53°), allowing continuous monitoring of moving space objects without the need for mechanical steering. The high gain and low phase error ensure accurate beam pointing and reliable detection performance at Ka-band frequencies.

For satellite communication and IoT-based global connectivity, the antenna supports spatial multiplexing by generating multiple independent beams, which can be used to establish simultaneous links with different satellites or users. This enhances system capacity, improves spectral efficiency, and enables reliable high-data-rate communication. Furthermore, the compact, low-loss GGW-based implementation makes the proposed design well suited for integration into next-generation 5G/6G satellite terminals and smart connectivity platforms.

Since the proposed structure operates at Ka-band frequencies, fabrication tolerance is an important practical consideration. The most sensitive parameters are the metallic pin dimensions of the GGW unit-cell, the coupling-region dimensions of the directional couplers, and the widths and lengths of the phase-shift compensators, since these directly affect the stopband behavior,

coupling ratios, and phase response. In practice, small machining deviations in these parameters may cause slight changes in return loss, coupling level, phase balance, and beam direction. Nevertheless, the close agreement between simulated and measured results demonstrates that the proposed beamforming network is sufficiently robust against practical fabrication and assembly tolerances.

IV. STATE-OF-THE-ART COMPARISON

To highlight the novelty and effectiveness of the proposed 3×3 GGW-based Nolen-Matrix Feeding Network (BNMFN), a comprehensive comparison is presented against recent beamforming architectures in terms of structural design, functional flexibility, and electrical performance.

A. Functional and Structural Comparison

Table V provides a comparative analysis of the proposed BNMFN with various existing beamforming networks based on key parameters, including feeding type, component integration, scanning dimensionality, operating frequency, number and type of phase shifters, and phase progression.

From Table V, it is evident that the proposed BNMFN employs a Nolen matrix structure using only couplers and phase shifters, similar to prior works [26,28]. However, compared with previously reported Nolen-matrix-based beamforming networks in [26] and [28], the proposed work introduces several key innovations in both design methodology and implementation.

First, the BNMFN is realized using groove gap-waveguide (GGW) technology at Ka-band (36–39 GHz), enabling a fully metallic, air-filled structure that significantly reduces dielectric and radiation losses, which are critical at millimeter-wave frequencies. Second, the proposed architecture eliminates conventional components such as power dividers, crossovers, switches, and terminations, and is implemented using only directional couplers and phase-shift compensators, resulting in a simplified and compact topology.

Furthermore, the design follows a systematic methodology in which the coupling ratios are derived from the equal-amplitude condition of the 3×3 Nolen matrix and translated into practical GGW coupler designs. These are combined with phase-shift compensators to achieve the desired phase distribution. In addition, the proposed BNMFN is validated as part of a fully integrated beamforming front-end, including an input feeding transition and a GGW-based slotted antenna array, demonstrating multi-beam operation at Ka-band frequencies.

Compared with [40], which is implemented using a printed structure at 5.8 GHz, the proposed work operates at significantly higher frequencies and addresses more challenging mm-wave requirements such as higher loss sensitivity, tighter fabrication tolerances, and stricter phase

accuracy. Moreover, while [40] relies on planar PCB technology, the proposed GGW-based implementation achieves inherently lower loss and higher efficiency.

Similarly, compared with Butler-matrix implementations in [41] and [42], which require multiple components such as crossovers, power dividers, and several phase shifters, the proposed 3×3 Nolen-matrix architecture achieves equivalent three-beam functionality using a reduced number of components. Specifically, the design employs only three directional couplers and two phase-shift compensators, eliminating crossovers, switches, and terminations. This results in a more compact, lower-complexity, and fabrication-friendly structure, particularly advantageous at mm-wave frequencies.

From a performance perspective, the proposed work demonstrates low insertion loss (≈5 dB), low phase error (~2°), and wideband operation (36–39 GHz), which are competitive with, and in some cases superior to, the reported results in [41]–[42], despite the reduced circuit complexity. Moreover, unlike [40]–[42], the proposed design is experimentally validated as a fully integrated beamforming front-end, achieving multi-beam radiation with gains exceeding 17 dBi.

While [41] and [42] focus on higher-order Butler matrices (e.g., 6×6 and 9×9) for multi-beam scalability, such architectures inherently introduce increased hardware complexity and routing challenges. In contrast, the proposed work is optimized for compact three-beam applications, providing a more efficient and practical solution for Ka-band satellite communications, space-multiplexing, and 6G IoT systems.

Finally, unlike many traditional matrix types such as Butler matrices [37,38] and parallel-fed networks [35,36], as well as closely related designs in [40]–[42], the proposed Nolen-matrix architecture inherently avoids crossover structures and requires fewer components, enabling efficient beamforming with reduced hardware complexity while supporting 3D beam scanning capability. Furthermore, the design achieves full 360° progressive phase shifting using only two continuously tuned phase shifters, minimizing hardware complexity and enhancing reconfigurability. This streamlined approach reduces system cost and power consumption while maintaining robust beamforming performance.

TABLE V. STATE-OF-THE-ART COMPARISON

Ref.	Feeding type	Components integration	Scanning dimension	Operating frequency (GHz)	Number of phase shifters	Shifting type	Phase shifting (°)	Progressive phase (°)

[26]	Nolen Matrix	Coupler, phase shifter	3D	0.921	3	Continuous	120	360
[28]	Nolen Matrix	Coupler, phase shifter	3D	5.8	3	Continuous	120	360
[40]	Three-way / Butler-like	Coupler	2D	5.8	0	Fixed	120	360
[41]	Butler Matrix	Coupler, phase shifter, crossover	2D	28	>6	Continuous	90-180	360
[42]	Butler Matrix	Coupler, phase shifter, crossover	2D	20-30	>6	Continuous	180	360
[35]	Parallel	Phase shifter, power divider, amplifier	2D	28	4	Switching	180	360
[36]	Parallel	Phase shifter, lumped element, divider	2D	2.5	4	Continuous	90	324
[37]	Butler Matrix	Coupler, phase shifter, power divider	2D	2.45	8	Switching	142	360
[38]	Butler Matrix	Coupler, phase	2D	2.4	6	Continuous	360	360

		shifter, crossover						
This Work	**Nolen-Matrix**	**Coupler, phase shifter**	**3D**	**38**	**2**	**Continuous**	**120**	**360**

B. Electrical Performance and Technology Comparison

Table VI outlines a technical performance comparison across recent beamforming matrix implementations, focusing on parameters such as fabrication technology, operating bandwidth, central frequency, reflection coefficient, transition coefficient, port isolation, and phase error.

The proposed BNMFN, based on GGW technology, achieves a 3 GHz bandwidth centred at 38 GHz, covering a critical segment of the Ka-band, which is increasingly important for high-data-rate satellite and 5G/6G wireless communications. Unlike earlier implementations operating at lower frequencies [27,39–41], the proposed design pushes the operational frequency to a higher mm-wave band while maintaining low loss and high performance.

In terms of reflection performance, the proposed network achieves a return loss of –20 dB, comparable to high-performance waveguide and SIW implementations [27,39]. Importantly, the transition coefficient of 5 dB is lower than those of most existing designs, indicating reduced insertion loss and improved power transfer efficiency. Additionally, the isolation between ports exceeds 20 dB, ensuring minimal crosstalk.

One of the most significant advantages is the low phase error of just 2°, demonstrating high accuracy in phase control an essential feature for precise beam steering and beamwidth control. This compares favourably against phase errors ranging from 5° to 11° in other technologies, as shown in Table VI.

By integrating the insights from Table IV and Table V, it is evident that the proposed GGW-based Nolen-Matrix Feeding Network delivers a unique balance of compactness, wide bandwidth, and low-loss performance, while also supporting 3D beam steering with minimal phase error and reduced hardware complexity.

These advantages make it an excellent candidate for next-generation mm-wave applications, particularly in satellite communications, space-multiplexing, and 5G/6G front-end systems, where performance, integration, and scalability are of paramount importance.

TABLE VI. STATE-OF-THE-ART COMPARISON II

Ref.	[27]	[39]	[43]	[44]	**This Work**

Feeding type	Nolen-Matrix	Butler-Matrix	Butler-Matrix	Butler-Matrix	**Nolen-Matrix**
Technology	Waveguide	SIW	Waveguide	Hollow Waveguide	**Groove Gap-Waveguide**
Bandwidth (GHz)	3	3	0.85	1	**3**
Frequency (GHz)	26	28	28	20	**38**
Reflection coefficient (dB)	-23	-30	-15	-23	**-20**
Transition coefficient (dB)	6.7	9.8	10	9	**5**
Isolation (dB)	25	25	25	20	**20**
Phase error (°)	5	11	9	6	**2**

V. CONCLUSION

This work presents an innovative and experimentally validated 3×3 beamforming Nolen-matrix feeding network (BNMFN) based on groove gap-waveguide (GGW) technology for Ka-band applications (36–39 GHz). The key contribution lies in the crossover-free architecture, realized using only directional couplers and phase-shift compensators, thereby eliminating conventional components such as power dividers, terminations, and crossovers that typically increase loss and complexity in traditional Blass and Butler matrix implementations.

The proposed BNMFN incorporates three 90° directional couplers with coupling ratios of 3.14 dB and 4.84 dB, along with two phase-shift compensators providing −63° and −38° phase shifts. This configuration enables the required output phase differences of 270°, 30°, and 150°, ensuring accurate multi-beam radiation. The system is validated across the 36–39 GHz band through integration with a custom-designed input feeding transition (IFT) and a three-element GGW-based slotted antenna array. The integrated front-end demonstrates stable radiation in three distinct directions with realized gains exceeding 17 dBi at 38 GHz.

Owing to its compact size, low insertion loss, reduced hardware complexity, and scalability, the proposed GGW-based BNMFN provides an efficient and practical solution for next-generation beamforming arrays, space-multiplexed systems, and 6G millimeter-wave satellite communication platforms, including applications in space target tracking and global connectivity.

ACKNOWLEDGMENT

Co-funded by the European Union. Views and opinions expressed are however those of the author(s) only and do not necessarily reflect those of the European Union or the European Research Executive Agency. Neither the European Union nor the granting authority can be held responsible for them. Besides that, this publication has emanated from research jointly funded by Taighde Éireann – Research Ireland under Grant number 13/RC/2094_2, the European Union's Marie Sklodowska-Curie Actions under grant number 101126578 and was supported in part by University of Galway. Besides that, the author extends the appreciation to the Deanship of Postgraduate Studies and Scientific Research at Majmaah University for funding this research work through the project number (R-2026-xxx).

REFERENCES

[1] Neetirajsinh J. Chhasatia, et al., "Compact spaced-dual-band filtering via ridge-gap waveguide for enhanced satellite communications", Results in Engineering, Volume 25, 104007, 2025.

[2] Mousa Abdollahvand et al., "Single-layer dual-band frequency selective surface for coverage-enhancing applications in millimeter-wave 5G", Results in Engineering, Volume 27, 105747, 2025.

[3] Wahaj Abbas Awan et al., "Compact and directional dual band antenna with low mutual coupling MIMO configuration for mm-wave communication", Results in Engineering, Volume 26, 105457, 2025.

[4] Md Ashraful Haque et al., "Machine learning-based technique for directivity prediction of a compact and highly efficient 4-port MIMO antenna for 5G millimeter wave applications", Results in Engineering, Volume 24, 103106, 2024.

[5] S. Chen et al., "Beam-Space Multiplexing: Practice, Theory, and Trends, From 4G TD-LTE, 5G, to 6G and Beyond," *IEEE Wireless Communications*, vol. 27, no. 2, pp. 162-172, 2020.

[6] M. Li, C. Han and S. Jin, "Hybrid Beamforming with Orthogonal Delay-Doppler Division Multiplexing Modulation for Terahertz Sensing and Communication," *IEEE Journal on Selected Areas in Communications*, doi: 10.1109/JSAC.2025.3610799.

[7] T. Liao, W. Guo, H. He, S. Song, J. Zhang and K. B. Letaief, "Joint Beamforming and Antenna Position Optimization for Fluid Antenna-Assisted MU-MIMO Networks," *IEEE Journal on Selected Areas in Communications*, doi: 10.1109/JSAC.2025.3615569.

[8] Duan, F.; Guo, Y.; Gu, Z.; Yin, Y.; Wu, Y.; Chen, T., "Optical Beamforming Networks for Millimeter-Wave Wireless Communications", Appl. Sci. 2023, 13, 8346.

[9] M. Ansari et al., "A highly efficient spherical Luneburg lens for low microwave frequencies realized with a metal-based artificial medium," *IEEE Transactions on Antennas and Propagation*, vol. 69, no. 7, pp. 3758–3770, Jul. 2021.

[10] J.-W. Lian et al., "Reduced-sidelobe multibeam array antenna based on SIW Rotman lens," *IEEE Antennas and Wireless Propagation Letters*, vol. 19, no.1, pp. 188–192, Jan. 2020.

[11] Y. J. Guo, M. Ansari et al., "Circuit Type Multiple Beamforming Networks for Antenna Arrays in 5G and 6G Terrestrial and Non-Terrestrial Networks," *IEEE Journal of Microwaves*, vol. 1, no. 3, pp. 704-722, July 2021.

[12] H. Zhu, et al., "Wideband Beam-Forming Networks Utilizing Planar Hybrid Couplers and Phase Shifters," *IEEE Transactions on Antennas and Propagation*, vol. 70, no. 9, pp. 7592-7602, Sept. 2022.

[13] Saeed MA and Nwajana AO, "A review of beamforming microstrip patch antenna array for future 5G/6G networks", *Frontiers in Mechanical Engineering*, Volume 9, 1288171, pp.1-15, February 2024.

[14] R.-J. Gong et al., "Circularly polarized multibeam antenna array of ME dipole fed by 5×6 Butler matrix," *IEEE Antennas and Wireless Propagation Letters*, vol. 18, no. 4, pp. 712–716, Apr. 2019.

[15] A. K. Vallappil et al., "Butler Matrix Based Beamforming Networks for Phased Array Antenna Systems: A Comprehensive Review and Future Directions for 5G Applications," *IEEE Access*, vol. 9, pp. 3970-3987, 2021.

[16] K. Xiang et al., "A broadband 3×4 Butler matrix and its application in multibeam antenna arrays," *IEEE Transactions on Antennas and Propagation*, vol. 67, no. 12, pp. 7622–7627, Dec. 2019.

[17] C. Qin, F.-C. Chen, and K.-R. Xiang, "A 5×8 Butler matrix based on substrate integrated waveguide technology for millimeter-wave multi-beam application," *IEEE Antennas and Wireless Propagation Letters*, vol. 20, no. 7, pp. 1292–1296, Jul. 2021.

[18] G. Buttazzoni *et al.*, "A Simple Blass Matrix Design Strategy for Multibeam Arbitrary Linear Antenna Arrays," *IEEE Transactions on Antennas and Propagation*, vol. 71, no. 11, pp. 8514-8524, Nov. 2023.

[19] Y. Yang et al., "Analytical Design Method and Implementation of Broadband 4 × 4 Nolen Matrix," *IEEE Transactions on Microwave Theory and Techniques*, vol. 70, no. 1, pp. 343-355, Jan. 2022.

[20] Tian-Gui Huang, Fu-Chang Chen, Jia-Zuo Cao, Kai-Ran Xiang, Yun Wang, "A tunable 3×5 Nolen matrix for sidelobe-reduced and beamforming applications", *AEU - International Journal of Electronics and Communications*, Volume 187, 155553, 2024.

[21] A. Tajik et al., "Asymmetrical 4×4 Butler matrix and its application for single layer 8×8 Butler matrix," *IEEE Transactions on Antennas and Propagation*, vol. 67, no. 8, pp. 5372–5379, Aug. 2019.

[22] H. Ren et al., "A novel 2-D 3×3 Nolen matrix for 2-D beamforming applications," *IEEE Transactions on Microwave Theory and Techniques*, vol. 67, no. 11, pp. 4622–4631, Nov. 2019.

[23] H. Zhu, P. Qin, and Y. J. Guo, "Single-ended-to-balanced power divider with extended common-mode suppression and its application to differential 2×4 Butler matrices," *IEEE Transactions on Microwave Theory and Techniques*, vol. 68, 563 no. 4, pp. 1510–1519, Apr. 2020.

[24] H. Zhang and B. Arigong, "Full 3D Coverage Beamforming Phased Array with Reduced Phase Shifters and Control 2D Tunable 3 × 3 Nolen Matrix," *IEEE International Symposium on Phased Array Systems & Technology (PAST)*, pp. 1-6, Waltham, MA, USA, 11-14 October 2022.

[25] Hussam Keriee, Mohamad Kamal A. Rahim, Osman Ayop, and Nawres Abbas Nayyef, "Beamforming networks using the Nolen matrix for 5G applications", *Waves in Random and Complex Media*, Feb 2023.

[26] Han Ren, Hanxiang Zhang, Bayaner Arigong, "Ultra-compact 3 × 3 Nolen matrix beamforming network", *IET Microwaves, Antennas & Propagation*, Vol. 14 Iss. 3, pp. 143-148, 2020.

[27] H. O. Hanoosh, M. K. A. Rahim, N. Asniza Murad and Y. Mahmood Hussein, "A 3×3 Antenna Beamforming Network Based on Waveguide Nolen Matrix for Ka-Bands," *IEEE Access*, vol. 12, pp. 151893-151906, 2024.

[28] G. Zhang, H. Yan, P. Liu, S. Z. Pour, and B. Arigong, "High-capacity multiple-input multiple-output communication for Internet-of-Things applications using 3D steering Nolen beamforming array," *Electronics*, vol. 13, no.13, p. 2452, 2024.

[29] P. Li, H. Ren and B. Arigong, "A Symmetric Beam-Phased Array Fed by a Nolen Matrix Using 180° Couplers," *IEEE Microwave and Wireless Components Letters*, vol. 30, no. 4, pp. 387-390, April 2020.

[30] Q. Li, J. Hirokawa, T. Tomura and N. J. G. Fonseca, "Two-Dimensional One-Body 3 × 3-Way Hollow-Waveguide Nolen Matrix Using a Two-Plane Unequal Division Coupler," *IEEE Transactions on Microwave Theory and Techniques*, vol. 72, no. 1, pp. 376-390, Jan. 2024.

[31] M. A. Fuentes-Pascual, M. Baquero-Escudero, M. Ferrando-Rocher, J. I. Herranz-Herruzo and A. Valero-Nogueira, "5x7 Nolen Matrix in K-Band Implemented in Rectangular Waveguide," *18th European Conference on Antennas and Propagation (EuCAP)*, pp. 1-5, Glasgow, United Kingdom, 17-22 March 2024.

[32] Y. Shi, *et al.,* "Gap Waveguide Technology: An Overview of Millimeter-Wave Circuits Based on Gap Waveguide Technology Using Different Fabrication Technologies," *IEEE Microwave Magazine*, vol. 24, no. 1, pp. 62-73, Jan. 2023.

[33] W. Y. Yong, et al., "An Overview of Recent Development of the Gap-Waveguide Technology for mmWave and Sub-THz Applications," *IEEE Access*, vol. 11, pp. 69378-69400, 2023.

[34] David M. Pozar, "Microwave Engineering, 4th Edition", ISBN: 978-0-470-63155-3, 752 pages, November 2011.

[35] Lee, A.; Kim, S.H.; Lee, D.M.; Kim, J.H.; Jang, T.H., "The Generalization of Stage-Reduced STPS for Low-Loss Unequal 1 × 4 Phased Array Architecture for 5G IoT Applications", *IEEE Internet Things J*. 2024, 11, 19978–19987.

[36] Kang, L.; Li, H.; Wang, X.; Zhou, J.; Huang, J., "Circular Polarization-Agile and Continuous Beam-Steerable Array Antenna using A Hybrid Design Approach", *IEEE Trans. Antennas Propag*. 2022, 70, 1541–1546.

[37] Chang, C.; Lee, R.; Shih, T., "Design of a Beam Switching/Steering Butler Matrix for Phased Array System", *IEEE Trans. Antennas Propag*. 2010, 58, 367–374.

[38] Chu, H.; Hoang, T.; Ji, K.; Ma, T., "A Phase Distribution Network Using 2 × 4 Butler Matrix for Linear/Planar Beam-Scanning Arrays", *IEEE Access* 2021, 9, 133438–133448.

[39] Q.-L. Yang, Y.-L. Ban, J.-W. Lian, Z.-F. Yu, and B. Wu, ''SIW Butler matrix with modified hybrid coupler for slot antenna array,'' *IEEE Access*, vol. 4, pp. 9561–9569, 2016.

[40] K. Ding, X. Fang, Y. Wang and A. Chen, "Printed Dual-Layer Three-Way Directional Coupler Utilized as 3 × 3 Beamforming Network for Orthogonal Three-Beam Antenna Array," IEEE Antennas and Wireless Propagation Letters, vol. 13, pp. 911-914, 2014, doi: 10.1109/LAWP.2014.2321971.

[41] C. Geng, J. -W. Lian, Y. J. Guo and D. Ding, "Millimeter-Wave Three-Layer Substrate-Integrated 9 × 9 Butler Matrix and Its Application to Wide-Angle Endfire Multibeam Metasurface Antenna," IEEE Transactions on Microwave Theory and Techniques, vol. 72, no. 4, pp. 2253-2266, April 2024, doi: 10.1109/TMTT.2024.3369040.

[42] C. Wei, Y. Liu, J. -W. Lian, C. Geng and D. Ding, "Millimeter-Wave Wide-Angle Ridge Gap Waveguide Multibeam Antenna Fed by 3-D Printing Butler Matrix," IEEE Transactions on Microwave Theory and Techniques, vol. 73, no. 9, pp. 5791-5802, Sept. 2025, doi: 10.1109/TMTT.2025.3562201.

[43] M. W. Almeshehe, N. A. Murad, M. K. A. Rahim, O. Ayop, F. Zubir, M. Z. A. A. Aziz, M. N. Osman, and H. A. Majid, "Low loss waveguide based Butler matrix with iris coupling control method for millimeter wave applications,'' *Waves Random Complex Media*, vol.33, no.2, pp. 372–392, Feb. 2021.

[44] T. Tomura, D.-H. Kim, M. Wakasa, Y. Sunaguchi, J. Hirokawa, and K. Nishimori, "A 20-GHz-band 64 × 64 hollow waveg uide two-dimensional Butler matrix,'' *IEEE Access*, vol. 7, pp. 164080–164088, 2019.

Declaration of Interests Statement

We would like to confirm that all authors do not have any conflict of interest for publishing our work